Colloid Polym Sci (2015) 293:1847–1853
DOI 10.1007/s00396-015-3613-9

SHORT COMMUNICATION

Multi-color luminescence of hybrids based with lanthanide functionalized zeolite A and titania

Lei Chen[1] · **Bing Yan**[1]

Received: 5 March 2015 / Revised: 19 April 2015 / Accepted: 22 April 2015 / Published online: 5 May 2015

Abstract A so-called inside-outside double modification path is used to functionalize zeolite A (ZA) with two kinds of luminescent lanthanide species (Eu^{3+}/Tb^{3+} complex of thenoyltrifluoroacetylacetone (TAA) and acetylacetone (AA), and lanthanide polyoxometalate ($NaLnW_{10}O_{36}{\cdot}32H_2O$ (LnW_{10}, Ln=Eu, Tb, Dy)) to prepare the multi-component hybrid materials. ZA is functionalized with Eu^{3+}/Tb^{3+} through ion exchange reaction, and then TTA/AA ligands are introduced through gas dispersion (ship in bottle) method to the inside channel or pore structure of ZA. On the other hand, another species, LnW_{10}, is fabricated onto the surface of ZA through ionic liquid (1-methyl-3-propionyloxy imidazolium bromide) coordinated to titania as linker. The prepared hybrids show the multi-color luminescence for different composition and excitation. The results provide a useful path to obtain multi-component lanthanide hybrids.

Keywords Hybrids · Lanthanide polyoxometalate · Lanthanide complex · Functionalized zeolite A · Ionic liquid · Luminescence

Introduction

Lanthanide ions are well known for their unique luminescent properties such as a broad spectral range (from ultraviolet to infrared region, especially and efficient narrow-width emission band in the visible region) and a long decay lifetime for various applications [1, 2]. Organic lanthanide complexes are well known to be the efficient luminescent species for the energy transfer between organic ligands and lanthanide emitters [3, 4]. However, they have so far been limited for practical application as phosphor materials or devices due to their poor stabilities under high temperature or moisture conditions and low mechanical strength. So it can be expected to investigate and develop lanthanide organic–inorganic hybrid materials [5]. In these hybrids, luminescent lanthanide species can be assembled with hosts such as silica or mesoporous silica, microporous zeolite, and polymer [6–10]. To date, typical paths are utilized to afford the special chemical linkage to construct lanthanide hybrids, which depend on the modification of organic ligands for lanthanide ions with crosslinking siloxane reagents [8–10]. The covalently grafting onto the host materials can be easily realized. On the other hand, for some hosts such as zeolites, the ion exchange is also an important path to functionalize them [6, 11]. Besides, ionic liquid compounds also can be utilized to behave as double functional linker to construct lanthanide hybrids [12, 13].

On the basis of the design and assembly of luminescent lanthanide hybrid materials, the strategy and path can also be applied to introduce other functional species besides lanthanide species, which leads to the multi-component assembly of hybrid materials [14]. Especially the photophysical properties of these hybrids can be integrated for different photofunctional units in the hybrid system. Certainly, different lanthanide species can be fabricated into one hybrid system to realize the luminescence tuning and integrating.

In this work, we put forward a so-called inside-outside double modification path of zeolite A (ZA), and two different lanthanide species (lanthanide complex and lanthanide polyoxmetallate) can be introduced the hybrid systems

Electronic supplementary material The online version of this article (doi:10.1007/s00396-015-3613-9) contains supplementary material, which is available to authorized users.

✉ Bing Yan
byan@tongji.edu.cn

[1] Department of Chemistry, Tongji University, Siping Road 1239, Shanghai 200092, China

together with titania and ionic liquids. The photophysical tuning of these hybrids are discussed in detail.

Experimental section

Materials

Zeolite A (ZA) crystals with chemical purity and high crystallinity were synthesized according to the reported procedure [15]. $Ln(NO_3)_3{\cdot}6H_2O$ (Ln=Eu, Tb, Dy) were obtained by dissolving their respective oxides in concentrated nitric acid (69.2 %). Thenoyltrifluoroacetylacetone (TAA) and acetylacetone (AA) acetylacetone, sodium hydroxide, and potassium hydroxide (Aladdin) were from Aladdin. Colloidal silica (40 %, Ludox HS-40, Sigma) and tetraisopropyltitanate($Ti(OCH(CH_3)_2)_4$) from Aladdin were used without further purification. All the other chemicals were analytically pure and purchased from China National Medicines Group and used as received.

The synthesis of ionic liquid compound 1-methyl-3-propionyloxy imidazolium bromide (IM^+Br^-)

Highly purified 1-methyl-3-propionyloxy imidazolium bromide (IM^+Br^-) was synthesized according to a previously reported procedure [16]. 3-Bromopropionic acid (100 mmol) was first dissolved in 10 mL absolute ethyl alcohol, and then an equal amount of substance 1-methyl imidazole was added to the solution stirred for 8 h at 348 K. The coarse product was washed with ether by three times and then taken down on a rotary evaporator to remove excess solvent to obtain a pale yellow ionic liquid, referred to as IM^+Br^-. The yield was 80 %. For IM^+Br^-: 1H NMR (400 MHz, DMSO-d^6): δ (9.25, s, 1H), δ (7.70, s, 1H), δ (7.60, s, 1H), δ (4.44, t, 2H), δ (2.92, t, 2H), δ (3.93, s, 3H).

Synthesis of four kinds of lanthanide polyoxometalates (LnW_{10})

$Na_9LnW_{10}O_{36}{\cdot}32H_2O$ ((LnW_{10})) can be abbreviated to LnW_{10} (Ln=Eu, Tb, Dy). The synthesis of POMs was prepared with the method reported by Peacock and Weakley [17]. First, 100 mmol of $Na_2WO_4{\cdot}2H_2O$ was dissolved in 10 mL deionized water, the solution was heated to 358 K, and then pH was adjusted to about 7–8 with glacial acetic acid. One-millimole aqueous solution of $Ln(NO_3)_3{\cdot}6H_2O$ (0.8 mL) was added to the solution dropwise by stirring. In the process of adding, a lot of white precipitate was immediately generated, and in the end, the heating and cooling to room temperature were stopped. The product was obtained by filtration and then dried under normal atmospheric conditions. The colorless crystals are LnW_{10} (Ln=Eu/Tb).

Preparation of TTA-Eu⊂ZA and AA-Tb⊂ZA

TTA-Eu⊂ZA and AA-Tb⊂ZA were synthesized according to the ion exchange reaction. ZA (100 mg) was stirred in 1.2 mL of a 0.05 M aqueous solution of $Eu(NO_3)_3{\cdot}6H_2O$ ($Tb(NO_3)_3{\cdot}6H_2O$) for 12 h at 353 K. The product was collected by centrifugation, washed with deionized water by three times, and then dried for 5 h at 353 K under normal atmospheric conditions. The organic–inorganic hybrid materials TTA-Eu⊂ZA and AA-Tb⊂ZA were synthesized by "ship in a bottle" method. After Eu⊂ZA and Tb⊂ZA were degassed and dried at 423 K for 2 h to get rid of the solvent molecules and water molecules, it was exposed to the TTA/AA vapor at 453/393 K for 18 h. The product was washed with CH_2Cl_2 by three times and dried at 333 K for 4 h under vacuum.

Preparation of TTA-Eu(AA-Tb)⊂ ZA-Ti-IM-LnW_{10}(Ln=Eu, Tb, Dy)

IM^+Br^- (0.9 mmol) was first suspended in 20 mL of ethanol solution; 0.1 mmol LnW_{10} was then added for ion exchange and refluxed in normal atmospheric conditions at 343 K for 24 h. $Ti(OCH(CH_3)_2)_4$ (0.9 mmol) and 100 mg ZA were added and refluxed at 343 K for another 6 h. Stop heating, 3.6 mmol deionized water was used to promote the hydrolysis reaction stirring at room temperature. The molar compositional ratio of the resulting gel was $1LnW_{10}/9IM/9Ti(OCH(CH_3)_2)_4/36H_2O$. The products were washed with anhydrous ethanol for three times and then dried for 10 h under vacuum.

Physical measurements

Fourier transform infrared (FTIR) spectra are measured within the 4000–400 cm^{-1} region on a Nexus 912 AO446 spectrophotometer with the KBr pellet technique. The X-ray powder diffraction (XRD) patterns are recorded on a Bruker D8 diffractometer (40 mA–40 kV) using monochromated Cu Ka1 radiation (k=1.54 Å) over the 2θ range of 10°–70° and 0.6°–6°. Scanning electronic microscope (SEM) images are obtained with a Philps XL-30. Luminescence excitation and emission spectra of the solid samples are obtained on Edinburgh FLS920 spectrophotometer. The outer luminescent quantum efficiency was measured using an integrating sphere (150-mm diameter, $BaSO_4$ coating) with the Edinburgh FLS920 phosphorimeter. The luminescence spectra were corrected for variations in the output of the excitation source and for variations in the detector response. The quantum yield was defined as the integrated intensity of the luminescence signal. Thermogravimetry (TG) data were measured on Netzsch STA 409C under nitrogen atmosphere by heating/cooling at the rate of 15 °C/min with the crucibles of Al_2O_3.

Results and discussion

Figure 1 shows the scheme of the composition and preparation process of multi-component hybrid system TTA-Eu(AA-Tb)⊂ZA-Ti-IM-LnW_{10}. First, Eu^{3+}(Tb^{3+}) functionalized zeolite A (Eu/Tb⊂ZA) is prepared by ion exchange reaction, which is degassed and dried under vacuum. Then, it is exposed to TTA/AA gas under vacuum vapor. In this process, the coordination reaction occurs between TTA/AA and Eu^{3+}/Tb^{3+} ion in ZA, resulting in the host–guest hybrid material TTA-Eu(AA-Tb)⊂ZA. On the other hand, LnW_{10} is linked to IM through the ion exchange reaction, resulting in IM-LnW_{10}. Then, IM-LnW_{10} is connected to titania by the chelating reaction between propionyloxy group of IM and $Ti(OCH(CH_3)_2)_4$. Finally, the final hybrids are assembled under mild conditions after hydrolysis and condensation process of $Ti(OCH(CH_3)_2)_4$ and hydroxyl groups onto the surface of ZA.

The morphology of ZA is the typical truncated cubes with an average dimension of 2 μm, whose structure of ZA material is visible in the scanning electron microscopy (SEM) picture in Supplementary Fig. S1 (top). After the preparation of ZA, all individual channels can be loaded with fitted dye molecules, leading to samples with obvious optical anisotropic properties on a macroscopic scale. The X-ray diffraction (XRD) pattern of ZA material is shown in Supplementary Fig. S1 (bottom), and the 2θ range of 5–70° for this measurement. Supplementary Fig. S2 shows the selected SEM image of the cylindrical structure of AA-Tb⊂ZA-Ti-IM-EuW_{10}TTA-Eu⊂ZA-Ti-IM-EuW_{10} (top) and AA-Tb⊂ZA-Al-IM-EuW_{10} (bottom). The crystal framework belonging to ZA still can be observed except for it becomes irregular as pure ZA for the introduction of other functionalized components in the hybrid system.

Figure 2 exhibits the selected FTIR spectra of hybrid materials (a) TTA-Eu⊂ZA-Ti-IM-EuW_{10}, (b) TTA-Eu⊂ZA-Ti-IM-TbW_{10}, (c) AA-Tb⊂ZA-Al-IM-EuW_{10}, and (d) AA-Tb⊂ZA-Al-IM-TbW_{10}. They are dominated by the intense anti-

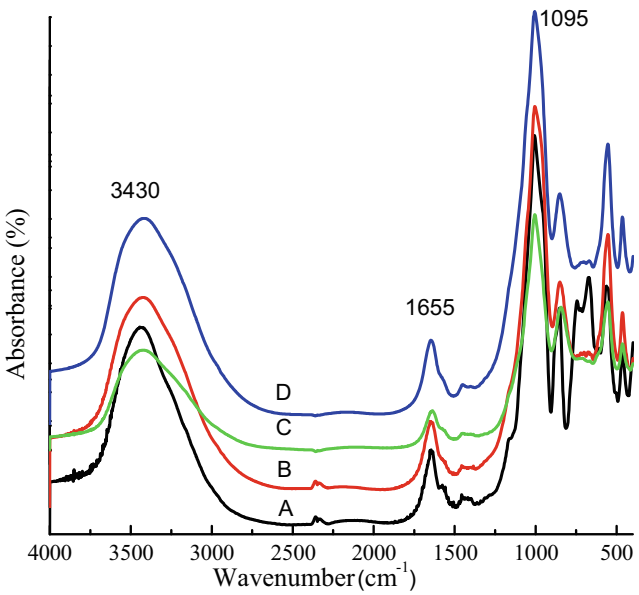

Fig. 2 The selected FTIR spectra of hybrid materials (**a**) TTA-Eu⊂ZA-Ti-IM-EuW_{10}, (**b**) TTA-Eu⊂ZA-Ti-IM-TbW_{10}, (**c**) AA-Tb⊂ZA-Ti-IM-EuW_{10}, and (**d**) AA-Tb⊂ZA-Ti-IM-TbW_{10}

symmetric V_{as} (M-O, M=Si, Al, or Ti) stretching vibrations at about 1095 cm^{-1}. The bands for the stretching and bending vibrations at 1200–400 cm^{-1} are corresponded to the ZA framework modes. The water molecules present in the materials are characterized by the stretching and the bending vibrations at about 3430 cm^{-1}. Furthermore, the C=O group of organic molecules present in the sample are characterized by the stretching vibration at 1655 cm^{-1} and can be easily recognized.

Figure 3 shows the luminescent excitation and emission spectra of lanthanide hybrids, for (a) TTA-Eu⊃ZA-Ti-IM-EuW_{10}, (b) TTA-Eu⊃ZA-Ti-IM-TbW_{10}, and (c) TTA-Eu⊃ZA-Ti-IM-DyW_{10}, respectively. For TTA-Eu⊃ZA-Ti-IM-EuW_{10} hybrids in Fig. 3a, the excitation spectra of them (200~500 nm) are obtained by monitoring the emission of Eu^{3+} ion at 613 nm, which shows the broad excitation band

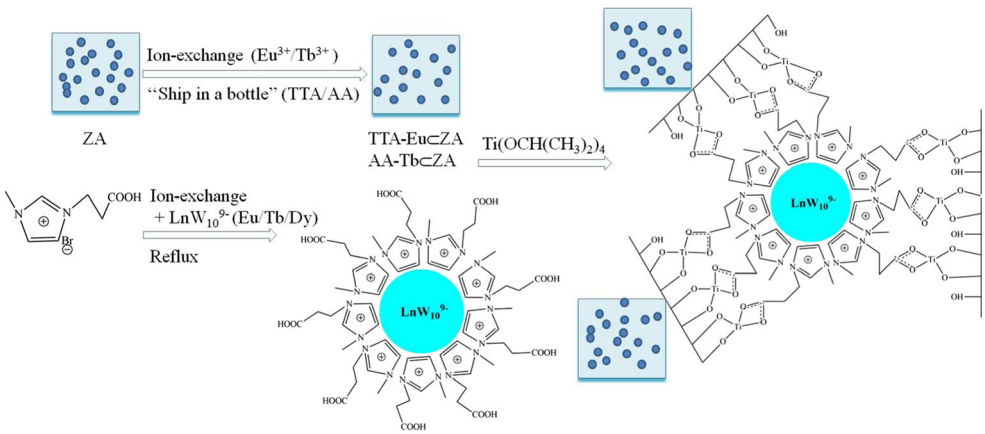

Fig. 1 The scheme for synthesis process and composition for the hybrid materials TTA-Eu(AA-Tb) ZA-Ti-IM-LnW_{10} (Ln=Eu, Tb, Dy)

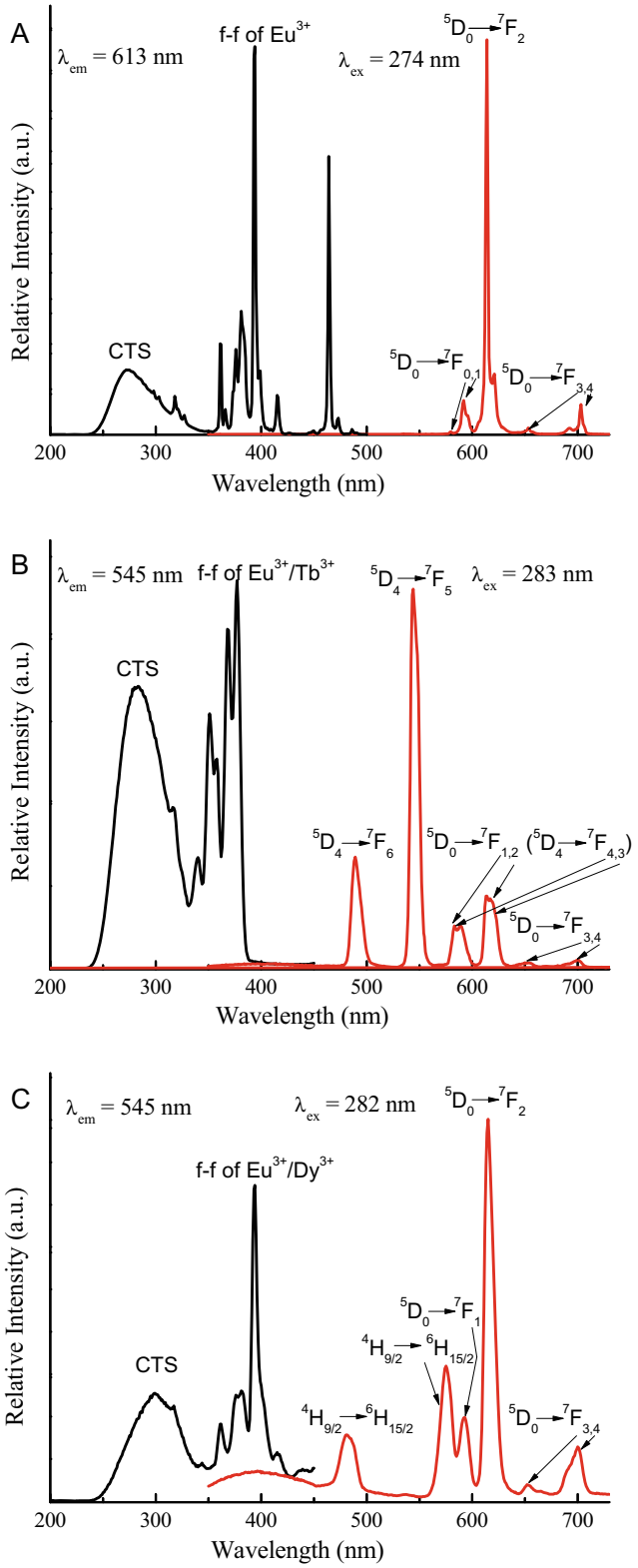

Fig. 3 The luminescence spectra of hybrid materials (**a**) TTA-Eu⊂ZA-Ti-IM-EuW_{10}, (**b**) TTA-Eu⊂ZA-Ti-IM-TbW_{10}, and (**c**) TTA-Eu⊂ZA-Ti-IM-DyW_{10}

ranging from 250 to 350 nm in the ultraviolet region, which is due to the formation of charge transfer state (CTS) band of Eu-O. Another shoulder band overlapping the wide excitation is due to the π-π^* electronic transitions of TTA coordinated to Eu^{3+}. Besides, the sharp excitation peak for f-f transition of Eu^{3+} is observed with stronger intensity, especially the transitions $^7F_0 \rightarrow {}^5L_6$ at 397 nm and $^7F_0 \rightarrow {}^5D_2$ at 466 nm. The corresponding emission spectral bands of the hybrids are assigned the $^5D_0 \rightarrow {}^7F_J$ (J=0–4) transitions at around 579, 591, 613, 622, and 700 nm under excitation at 274 nm [18]. Within the $^5D_0 \rightarrow {}^7F_2$ transition is the strongest emission at about 613 nm, which is different from the parent EuW_{10} with strong intensity of $^5D_0 \rightarrow {}^7F_1$ transition. The hybrid system consists of both Eu-TTA and EuW_{10}, resulting in the different emission performance from single EuW_{10}. But, we still can find the emission feature of EuW_{10}, whose luminescent band is apparent for $^5D_0 \rightarrow {}^7F_4$ transition in Fig. 3a. Figure 3b shows the excitation and emission spectra of hybrid TTA-Eu⊃ZA-Ti-IM-TbW_{10}. When the emission wavelength at 545 nm for Tb^{3+} is selected to measure the excitation

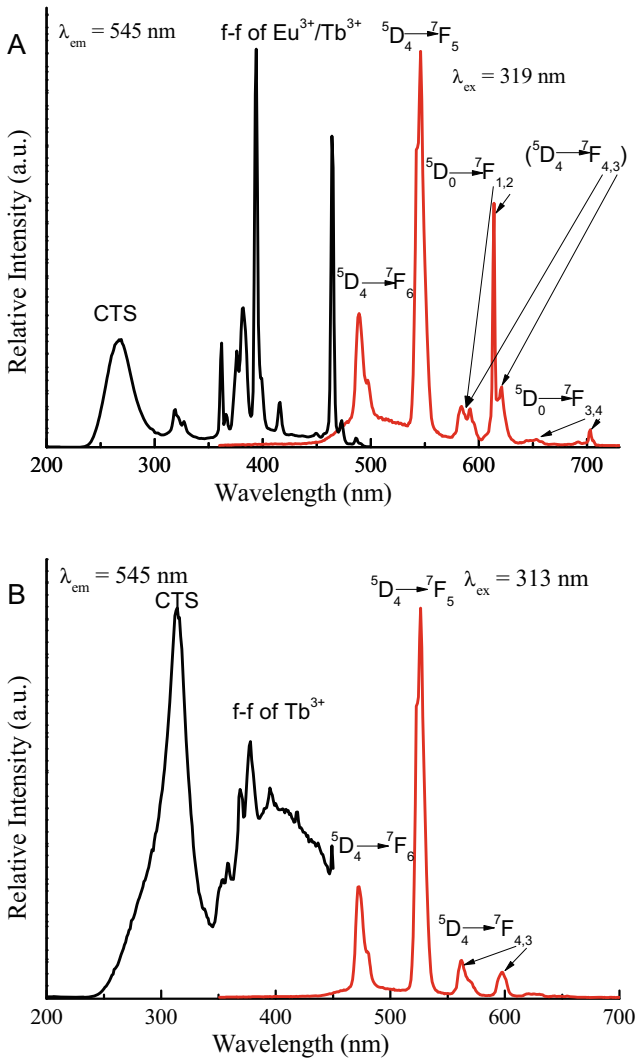

Fig. 4 The luminescence spectra of hybrid materials (**a**) AA-Tb⊂ZA-Al-IM-EuW_{10} and (**b**) AA-Tb⊂ZA-Ti-IM-TbW_{10}

spectrum, it presents the wide band ranging in 250~350 nm for the CTS Eu-O. Besides, some weak excitation lines of f-f transition for Eu^{3+} and Tb^{3+} at long wavelength 350–500 nm can be observed from the excitation spectrum, among which the f-f transitions (397 nm for $^7F_0 \rightarrow {}^5L_6$ and 466 nm for $^7F_0 \rightarrow {}^5D_2$) for Eu^{3+} possess the strong excitation intensity [18]. The characteristic emissions of the two lanthanide ions appear in Fig. 5. The two peaks at 490 and 544 nm are for the $^5D_4 \rightarrow {}^7F_6$ and $^5D_4 \rightarrow {}^7F_5$ transitions of Tb^{3+} [19]. Another two peaks at 650 and 700 nm are for $^5D_0 \rightarrow {}^7F_3$ and $^5D_0 \rightarrow {}^7F_4$ transitions of Eu^{3+}. The remaining two emission peaks at around 590 and 618 nm are mainly from $^5D_0 \rightarrow {}^7F_J$ (J=0, 1, 2) transition of Eu^{3+}, overlapped with the $^5D_4 \rightarrow {}^7F_6$ and $^5D_4 \rightarrow {}^7F_5$ transitions of Tb^{3+}. This is clearly seen from the width and ref-shift of the emission band at maximum of 618 nm. Figure 3c shows the excitation and emission spectrum of TTA-Eu⊃ZA-Ti-IM-DyW_{10} hybrids. The excitation spectrum monitored at 615 nm shows essentially broad band centered at about 200~450 nm. Among the wide excitation band at the range of 230–350 nm is mainly originated from the DyW_{10} unit and Eu-TTA to form charger transfer state (CTS) of Eu-O. Besides, some weak excitation lines of f-f transition for Eu^{3+} and Tb^{3+} at long wavelength of 350–500 nm can be observed to overlap with the excitation of host. The emission spectrum of TTA-Eu⊃ZA-Ti-IM-DyW_{10} is measured with excitation wavelength of 282 nm. The characteristic sharp bands at 485 and 575 nm, and 590, 615, 650, and 700 nm can be observed, which are ascribed to f-f transitions of Dy^{3+} ($^6H_{9/2}$–^6H_J, J=15/2, 13/2) and Eu^{3+} ($^5D_0$–^7F_J, J=0–4), respectively [20]. This indicates that Eu-TTA and DyW_{10} are both functionalized to the hybrid system.

Figure 4a shows the excitation and emission spectrum of AA-Tb⊂ZA-Ti-IM-EuW_{10} hybrids. The excitation spectrum monitored at 545 nm shows essentially broad band centered at about 200~500 nm. Among the wide excitation band at the range of 230–320 nm is mainly originated from the EuW_{10} unit to form charger transfer state (CTS) of Eu-O. Another shoulder band overlapping the wide excitation is due to the π-π^* electronic transitions of AA coordinated to Tb^{3+}. Besides, some weak excitation lines of f-f transition for Eu^{3+} and Tb^{3+} at long wavelength 350–500 nm can be observed from the excitation spectrum, among which the f-f transitions (397 nm for $^7F_0 \rightarrow {}^5L_6$ and 466 nm for $^7F_0 \rightarrow {}^5D_2$) for Eu^{3+} possess the strong excitation intensity [17]. The emission spectrum of AA-Tb⊂ZA-Ti-IM-EuW_{10} is measured with excitation wavelength of 319 nm. The characteristic sharp bands at 489 and 545 nm, and 580, 590 (595), 615 (620), 650, and 700 nm can be observed, which are ascribed to f-f transitions of Tb^{3+} ($^5D_4$–^7F_J, J=6, 5) and Eu^{3+} ($^5D_0$–^7F_J, J=0–4), respectively [20]. This indicates that Tb-AA and EuW_{10} are both functionalized to the hybrid system. Among the emission bands at around 590 (595) and 615 (620) nm belong to the

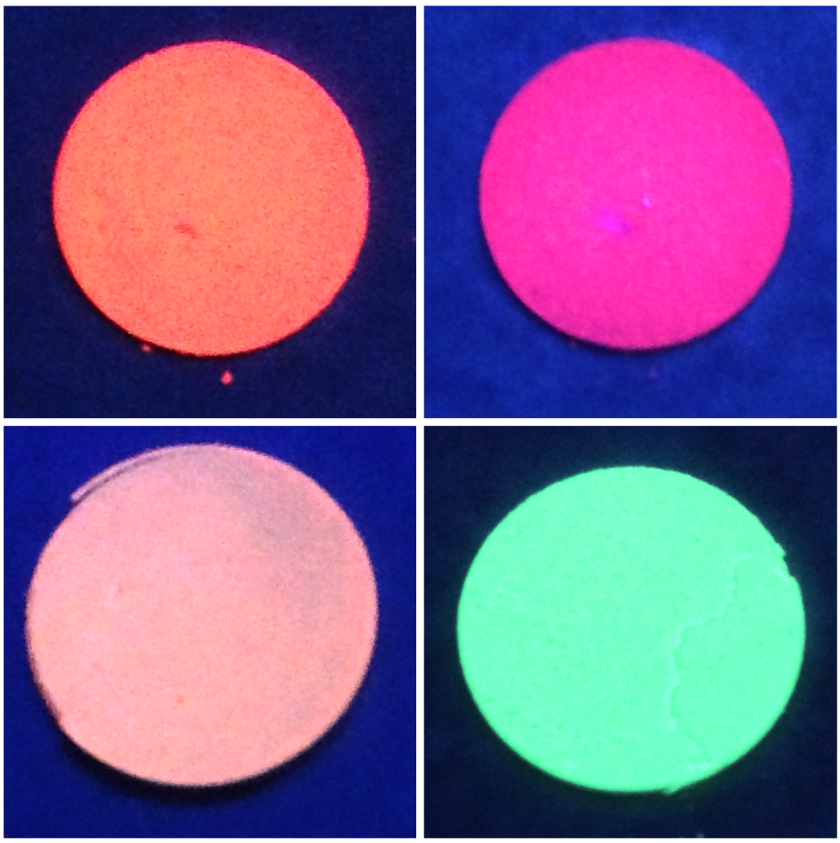

Fig. 5 The selected digital photos of hybrid materials TTA-Eu⊂ZA-Ti-IM-EuW_{10} (*top*) and AA-Tb⊂ZA-Ti-IM-EuW_{10} (*bottom*) under UV irradiation (λ_{ex}=254 nm for left; 365 nm for right)

overlap of both Eu^{3+} ($^5D_0$–$^7F_{1,2}$) and Tb^{3+} ($^5D_4$–$^7F_{4,3}$) transitions. It is worth pointing out that $^5D_0$–$^7F_0$ transition exhibits stronger intensity than $^5D_0$–$^7F_1$ one, which is different the character of parent EuW_{10} with high $^5D_0$ - $^7F_1$ emission. This may be due to two reasons: One is the introduction of other units in the hybrids, resulting in the different environment from parent EuW_{10}. The other is the overlap from the emission to the Tb^{3+} ($^5D_4$–$^7F_{4,3}$) transitions ($^5D_4$–$^7F_{4,3}$). Figure 4b shows the excitation and emission spectra of AA-Tb⊂ZA-Ti-IM-TbW_{10} hybrids. The excitation spectrum of monitored at 545 nm shows essentially broad band centered at about 250~450 nm. Among the wide excitation band at the range of 250–350 nm is mainly due to the absorption of TbW_{10} host together with π-π^* electronic transitions of AA, both of which behave as the energy donor for the luminescence of Tb^{3+}. Meanwhile, some weak sharp excitation peaks for the f-f transition of Tb^{3+} at long wavelength 350–450 nm can be observed. The corresponding emission spectrum of AA-Tb⊂ZA-Ti-IM-TbW_{10} is measured with excitation wavelength of 313 nm. The characteristic sharp bands at 490, 545, 590, and 620 nm can be observed, which are ascribed to f-f transitions of Tb^{3+} ($^5D_4$–^7F_J, J=6, 5, 4, 3). It is worth pointing out that $^5D_4$–$^7F_5$ transition exhibits the extremely stronger intensity than other transitions, which is the feature of TbW_{10} unit. The final hybrids show the green color emission.

Figure 5 shows the selected digital photos of hybrid materials TTA-Eu⊂ZA-Ti-IM-EuW_{10} (top), and AA-Tb⊂ZA-Al-IM-EuW_{10} (bottom) under UV irradiation (λ_{ex}=254 nm for left; 365 nm for right). For TTA-Eu⊂ZA-Ti-IM-EuW_{10} hybrids, under the UV irradiation of short wavelength 254 nm and long wavelength 365 nm, the color of the hybrids changes from orange-red to violet-red. This is due to the different dominant europium luminescent species. More apparent for AA-Tb⊂ZA-Al-IM-EuW_{10} hybrids, its color changes from light purple-red to light blue-green. So the selectively excitation of hybrids can realize the color tuning for the two luminescent species. Besides, the luminescent quantum yields of the five hybrid materials are determined, which are 49 % for TTA-Eu⊂ZA-Ti-IM-EuW_{10}, 40 % for TTA-Eu⊂ZA-Ti-IM-TbW_{10}, 25 % for TTA-Eu⊂ZA-Ti-IM-DyW_{10}, 43 % for AA-Tb⊂ZA-Al-IM-EuW_{10}, and 33 % for AA-Tb⊂ZA-Ti-IM-TbW_{10}, respectively.

Conclusions

In summary, Eu/Tb complex and lanthanide (Eu, Tb, Dy) polyometallates (LnW_{10}) are introduced to functionalize zeolite A and titania by an inside-outside double modification path. Eu/Tb complex modified zeolite A (TTA-Eu(AA-Tb)⊂ZA) is achieved by ionic exchange reaction and gas dispersion. LnW_{10} modified titania (Ti-IM-LnW_{10}) is obtained through ionic liquid compound as linker. Then, multi-component hybrids TTA-Eu(AA-Tb)⊂ZA-Ti-IM-LnW_{10} are assembled through condensation reaction between surface hydroxyl groups onto ZA and titania. The prepared hybrids show the red and green luminescence, which provides a useful path to obtain multi-component lanthanide hybrids.

Acknowledgments This work is supported by the National Natural Science Foundation of China (91122003) and Developing Science Fund of Tongji University.

References

1. BunzliJ CG, Piguet C (2005) Taking advantage of luminescent lanthanide ions. Chem Rev 34:120–132
2. Gawryszewska P, Sokolnicki J, Legendziewicz J (2005) Photophysics and structure of selected lanthanide compounds. Coord Chem Rev 249:2489–2509
3. Bunzli CG, Piguet C (2002) Lanthanide-containing molecular and supramolecular polymetallic functional assemblies. Chem Rev 102: 1897–1928
4. dos Santos GCM, Harte AJ, Quinn SJ, Gunnlaugsson T (2008) Recent developments in the field of supramolecular lanthanide luminescent sensors and self-assemblies. Coord Chem Rev 252: 2512–2527
5. Yan B (2012) Recent progress on photofunctional lanthanide hybrid materials. RSC Adv 2:9304–9324
6. Cao PP, Li HR, Zhang PM, Calzaferri G (2011) Self-assembling zeolite crystals into uniformly oriented layers. Langmuir 27:12614–12620
7. Feng J, Song SY, Fan WQ, Sun LN, Guo XM, Peng CY, Yu JBYN, Zhang HJ (2009) Near-infrared luminescent mesoporous MCM-41 materials covalently bonded with ternary thulium complexes. Microp Mesop Mater 117:278–284
8. Li YJ, Wang L, Yan B (2011) Photoactive lanthanide hybrids covalently bonded to functionalized periodic mesoporous organosilica (PMO) by calix[4]arene derivative. Mater Chem 21: 1130–1138
9. GuY J, Yan B (2013) Lanthanide mesoporous SBA-15 hybrids through functionalized 6-hydroxybenz[de]anthracen-7-one linkage: UV-visible light sensitization and visible-NIR luminescence. J Coll Interf Sci 393:36–43
10. GuY. J., B. Yan (2013) Novel photoconversion lanthanide functionalized SBA-15 mesoporous hybrids: ultraviolet–visible excitation and visible-NIR emission.*Eur. J. Inorg. Chem.* 2963–2970.
11. Hao JN, Yan B (2014) Photofunctional host-guest hybrid materials and thin film of lanthanide complexes covalently linked to functionalized Zeolite A. Dalton Trans 43:2810–2818
12. Li QP, Yan B (2012) Luminescent hybrid materials of Lanthanide β-diketonate and mesoporous host through the covalent and ion bonding with anion metathesis. Dalton Trans 41:8567–8574
13. Mei Y, Lu Y, Yan B (2013) Multi-component hybrid soft gels containing Eu^{3+} complexes and MS (M = Zn, Cd) nanoparticles assembled with mercapto- ion liquid linkage: adjustable color and white luminescence. New J Chem 37:2619–2623
14. Laine P, Seifert R, Giovanoli R, Calzaferri G (1997) convenient preparation of close-packed monograin layers of pure zeolite A microcrystals. New J Chem 21:453–460
15. Chen L, Yan B (2014) Multi-component assembly and luminescence tuning of lanthanide hybrids based with both Zeolite L/A

and SBA-15 through two organically grafted linkers. Dalton Trans 43:14123–14131

16. Gomez E, Gonzalez B, Dominguez A, Tojo E, Tojo J (2006) Dynamic viscosities of a series of 1-alkyl-3-methylimidazolium chloride ionic liquids and their binary mixtures with water at several temperatures. J Chem Eng Data 51:696–701
17. Peacock R. D., T. J. R. Weakley (1971) Heteropolytungstate complexes of the lanthanide elements. Part I. Preparation and reactions. *J. Chem. Soc. (A)*1836–1839.
18. Carnall WT, Fields PR, Rajnak K (1968) Electronic energy levels of the trivalent lanthanide aquo ions. IV. Eu^{3+}. J Chem Phys 49:4450
19. Carnall WT, Fields PR, Rajnak K (1968) Electronic energy levels of the trivalent lanthanide aquo ions. III. Tb^{3+}. J Chem Phys 49:4447
20. Carnall WT, Fields PR, Rajnak K (1968) Electronic energy levels of the trivalent lanthanide aquo ions. I. Pr^{3+}, Nd^{3+},Pm^{3+},Sm^{3+},Dy^{3+}, Ho^{3+}, Er^{3+}, Tm. J Chem Phys 49:4424